iScience

CellPress
OPEN ACCESS

Article

Arhgef2 regulates neural differentiation in the cerebral cortex through mRNA m^{6}A-methylation of Npdc1 and Cend1

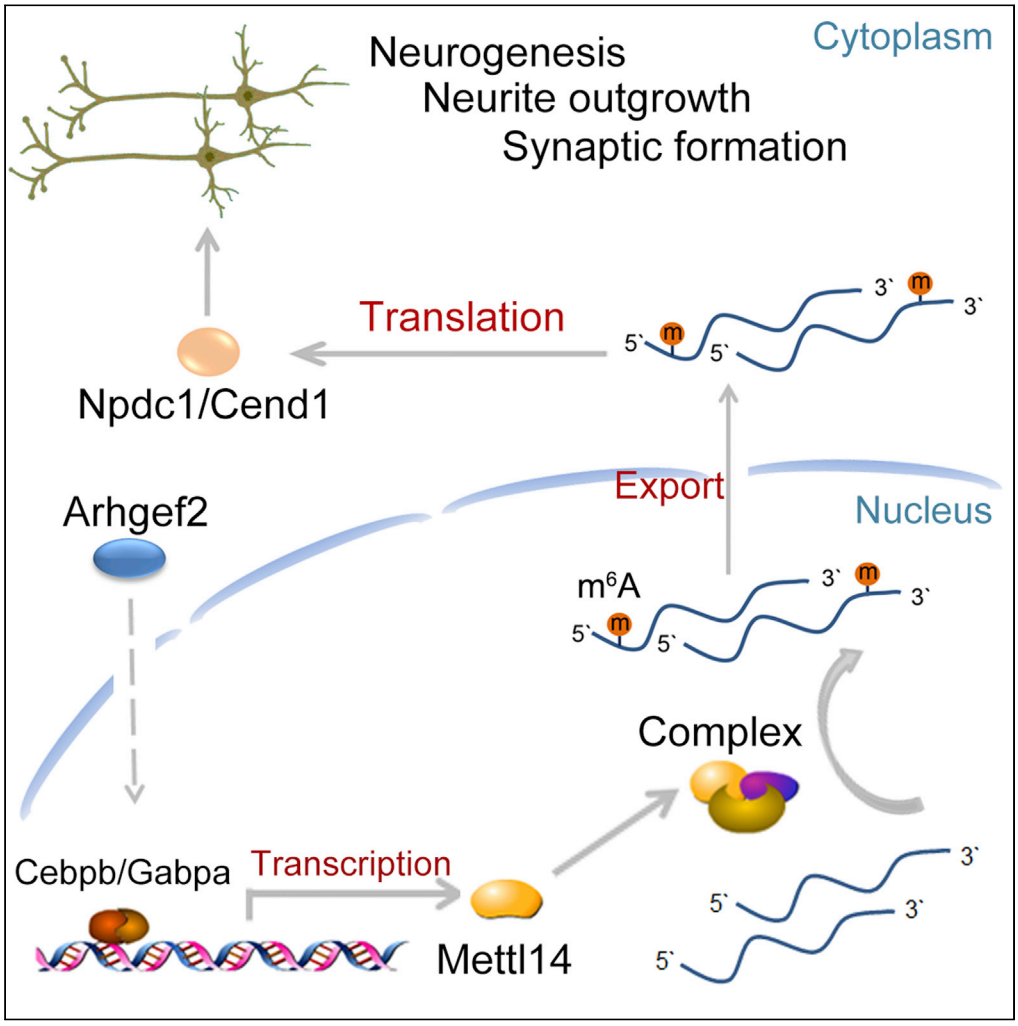

Pei Zhou, Yifei Qi, Xiang Fang, ..., Na Li, Angela M. Kaindl, Hao Hu

eddy3207@126.com (Y.Q.)
huh@cougarlab.org (H.H.)

Highlights

Arhgef2 mediates total m^{6}A level via Mettl14

Arhgef2 affects m^{6}A methylations of the *Npdc1* and *Cend1* mRNAs

Decreased m^{6}A methylations inhibits translation of Npdc1 and nuclear export of Cend1

Reduced protein expression of Npdc1 and Cend1 hinders neural differentiation

Zhou et al., iScience *24*, 102645
June 25, 2021
https://doi.org/10.1016/j.isci.2021.102645

iScience

CellPress
OPEN ACCESS

Article

Arhgef2 regulates neural differentiation in the cerebral cortex through mRNA m^{6}A-methylation of Npdc1 and Cend1

Pei Zhou,[1,11] Yifei Qi,[2,11,*] Xiang Fang,[1] Miaomiao Yang,[1] Shuxin Zheng,[1] Caihua Liao,[1] Fengying Qin,[1] Lili Liu,[1] Hong Li,[1] Yan Li,[1] Ethiraj Ravindran,[3,4,5] Chuanbo Sun,[1] Xinshu Wei,[1,6] Wen Wang,[7] Liang Fang,[7] Dingding Han,[1] Changgeng Peng,[8] Wei Chen,[7] Na Li,[1] Angela M. Kaindl,[3,4,5] and Hao Hu[1,6,9,10,12,*]

SUMMARY

N^6-methyladenosine (m^6A) is emerging as a vital factor regulating neural differentiation. Here, we report that deficiency of *Arhgef2*, a novel cause of a neurodevelopmental disorder we identified recently, impairs neurogenesis, neurite outgrowth, and synaptic formation by regulating m^6A methylation. *Arhgef2* knockout decreases expression of *Mettl14* and total m^6A level significantly in the cerebral cortex. m^6A sequencing reveals that loss of *Arhgef2* reduces m^6A methylation of 1,622 mRNAs, including *Npdc1* and *Cend1*, which are both strongly associated with cell cycle exit and terminal neural differentiation. *Arhgef2* deficiency decreases m^6A methylations of the *Npdc1* and *Cend1* mRNAs via down-regulation of Mettl14, and thereby inhibits the translation of *Npdc1* and nuclear export of *Cend1* mRNAs. Overexpression of Mettl14, Npdc1, and Cend1 rescue the abnormal phenotypes in *Arhgef2* knockout mice, respectively. Our study provides a critical insight into a mechanism by which defective *Arhgef2* mediates m^6A-tagged target mRNAs to impair neural differentiation.

INTRODUCTION

ARHGEF2 (synonym GEF-H1, murine Lfc), a member of the Rho guanine nucleotide exchange factor family, is crucial for controlling the spatiotemporal activation of Rho GTPases (Ren et al., 1998; Krendel et al., 2002). It is now well established that *ARHGEF2* controls microtubule dynamics through RhoA activation (Meiri et al., 2012; Birkenfeld et al., 2007; Tonami et al., 2011). Lack of *ARHGEF2* is strongly associated with an alternation in the organization of the actin cytoskeleton at the cell edge (Nalbant et al., 2009). *ARHGEF2* is required for mitotic spindle formation and orientation (Bakal et al., 2005; Yoshizaki et al., 2004). Recently, we successfully linked *ARHGEF2* to neurologic disease by reporting a homozygous *ARHGEF2* mutation in individuals with a neurodevelopmental phenotype including brain malformation (Ravindran et al., 2017). *ARHGEF2* loss of function impaired neuronal migration by RhoA/ROCK/MLC pathway, which caused the abnormal location of precerebellar neurons in the hindbrain (Ravindran et al., 2017). Although we found that defective *ARHGEF2* resulted in reduced neurogenesis of neocortical progenitors and probably contributed to microcephaly phenotype, little is known about whether *ARHGEF2* regulates neurite outgrowth and synaptic formation during neural differentiation. Thus, the molecular mechanism that how *ARHGEF2* mediates neural differentiation of brain cortex needs to be further investigated.

Dynamic methylation at the N^6 site of adenosine (N^6-methyladenosine, m^6A) has been indicated as the most prevalent internal mRNA modification in eukaryotes (Zhuang et al., 2019). A growing body of evidence has revealed that 0.1%–0.4% of all adenosines in mammal transcripts are modified by m^6A, which enriched in long exons, near transcription start sites, and stop codons (Meyer and Jaffrey, 2014; Wang and Zhao, 2016). It is involved in various biological processes, including mRNA splicing, localization, stability, and translation (Haussmann et al., 2016; Roundtree et al., 2017; Wang et al., 2014; Li et al., 2017). In recent years, m^6A is emerging as a key factor regulating neural differentiation. Deficiency of methyltransferase-like Mettl14 leads to the reduced nuclear export of m^6A-modified mRNAs regulating neural differentiation (Edens et al., 2019). Depletion of m^6A by *Mettl14* knockout in embryonic mouse brains prolongs the cell cycle of radial glia cells and extends cortical neurogenesis into postnatal stages (Yoon et al., 2017), phenocopying *Arhgef2* knockout mice we constructed in this

[1]Laboratory of Medical Systems Biology, Guangzhou Women and Children's Medical Center, Guangzhou Medical University, 510623 Guangzhou, China

[2]Division of Uterine Vascular Biology, Guangzhou Women and Children's Medical Center, Guangzhou Medical University, 510623 Guangzhou, China

[3]Charité - Universitätsmedizin Berlin, Institute of Cell Biology and Neurobiology, Berlin, Germany

[4]Charité - Universitätsmedizin Berlin, Department of Pediatric Neurology, Berlin, Germany

[5]Charité - Universitätsmedizin Berlin, Center for Chronically Sick Children, Berlin, Germany

[6]School of Medicine, South China University of Technology, 510006 Guangzhou, China

[7]Shenzhen Key Laboratory of Gene Regulation and Systems Biology, School of Life Sciences and Academy for Advanced Interdisciplinary Studies, Southern University of Science and Technology, Shenzhen 518005, China

[8]The First Rehabilitation Hospital of Shanghai, Tongji University School of Medicine, 200029 Shanghai, China

[9]Guangdong Provincial Key Laboratory of Research in Structural Birth Defect Disease, Guangzhou Women and Children's Medical Center, Guangzhou Medical University, 510623 Guangzhou, China

[10]Third Affiliated Hospital of Zhengzhou University, 450052 Zhengzhou, China

Continued

study. Furthermore, in view of drastically increased m^{6}A levels in adult mouse brain compared with embryogenesis period (Meyer et al., 2012), it remains possible that m^{6}A modification plays a unique role in the adult brain. Indeed, a compelling evidence points out that deletion of *Mettl14* in the adult brain severely impairs learning and performance, which is correlated to protein synthesis in synapses of striatum (Koranda et al., 2018). However, the mechanism of m^{6}A modification on neurite outgrowth and synaptic formation in postnatal brain cortex is still covered with a mysterious veil.

In this study, we cross-linked the function of *Arhgef2* and modification of m^{6}A regulated by *Mettl14*. The anomaly of neurogenesis, neurite outgrowth, and synaptic formation was demonstrated in an *Arhgef2* knockout mouse model. We further illustrated the function of *Mettl14* in this process and investigated underlying cellular and molecular mechanisms. Together, our data revealed a vital role of *Arhgef2* in regulating neural differentiation by m^{6}A-modified target mRNAs.

RESULTS

Defective *Arhgef2* caused microcephaly in adult mice

Previously, we reported a homozygous *ARHGEF2* mutation in individuals with a neurodevelopmental phenotype including brain malformation (Ravindran et al., 2017). To explore the pathomechanism of brain malformation by loss of *Arhgef2*, we constructed an *Arhgef2* knockout (*Arhgef2*−/−) mice model using *CRISPR-Cas9* genome editing technology (Figure S1). A 1.14-fold decrease in brain weight was noted in response to *Arhgef2* knockout, whereas the body weight had no significant change. Compared with wild-type littermates, the brain size was significantly decreased in *Arhgef2*−/− mice (Figure 1A). Nissl staining further exhibited reduced thickness of frontal and motor cortex in *Arhgef2*−/− mice (Figure 1B).

Defective *Arhgef2* led to abnormality of neural differentiation

Our recent study indicated that, in mouse neocortex, *Arhgef2* regulates neurogenesis from cortical precursor cells (Ravindran et al., 2017). As we expected, the number of NeuN$^+$ cells significantly decreased in *Arhgef2*−/− mice brain cortex compared with wild-type mice (postnatal 8 weeks), and it showed no tendency at all layers (Figure 2A). To test whether the genetic removal of *Arhgef2* affects neurite branching and synapse formation during neural differentiation, we examined the morphology of cortical neurites and dendrite spines in adult *Arhgef2*−/− mice. Golgi staining demonstrated that the spine density and length were significantly below the level of those of wild-type mice, with obviously abnormal morphology of neurites. Moreover, mature spines, which are characterized by mushroom-like shape, significantly reduced in *Arhgef2*−/− mice compared with wild-type mice (Figures 2B and 2C). We also analyzed the expression of presynaptic protein Synaptophysin and postsynaptic protein Psd-95. Compared with wild-type mice, expression of Psd-95 decreased in *Arhgef2*−/− mice (Figure 2D), whereas Synaptophysin showed no significant change (data not shown).

Genetic deletion of *Arhgef2* reduced m^{6}A level in brain cortex

The present studies provided strong evidence that m^{6}A deficiency in brain disrupted genes related to neuronal differentiation and impaired learning behaviors (Edens et al., 2019; Merkurjev, 2018; Koranda et al., 2018). To explore whether deficiency of *Arhgef2* affects m^{6}A level, we measured total m^{6}A level of adult mouse brain cortex and the expression of writer and eraser genes involved in m^{6}A methylation and demethylation. In *Arhgef2*−/− mice, total m^{6}A level significantly decreased compared with wild-type mice. Meanwhile, mRNAs of methylases *Mettl3* and *Wtap* showed a slight reduction without significance, whereas *Mettl14*, a vital factor controlling neural differentiation (Yoon et al., 2017), showed an observable downregulation. Demethylases *Fto* and *Alkbh5* showed no observable change (Figures 3A–3C and S2A). Furthermore, we found *Cebpb* and *Gabpa*, transcription factors binding at the transcription start site of Mettl14, were significantly decreased in *Arhgef2*−/− mice compared with wild-type mice, whereas *Cebpa*, *Elf1*, and *Spi1* showed no significant change (Weng et al., 2018) (Figures 3D and S2B). In parallel, Gene Set Enrichment Analysis (GSEA) of bulk RNA sequencing showed that the m^{6}A-associated genes (writers, erasers, readers, *Cebpb*, and *Gabpa*) were significantly enriched in the downregulated genes of *Arhgef2*−/− mice (Figure 3E).

Loss of *Arhgef2* inhibited the translation or nuclear export of m^{6}A-tagged *Npdc1* and *Cend1* mRNAs related to neural differentiation

To explore how the deficiency of *Arhgef2* affects neural differentiation by m^{6}A modification, we performed m^{6}A immunoprecipitation followed by RNA sequencing (m^{6}A-seq). Similar patterns of the total m^{6}A distribution in

[11]These authors contributed equally

[12]Lead contact

*Correspondence: eddy3207@126.com (Y.Q.), huh@cougarlab.org (H.H.)

https://doi.org/10.1016/j.isci.2021.102645

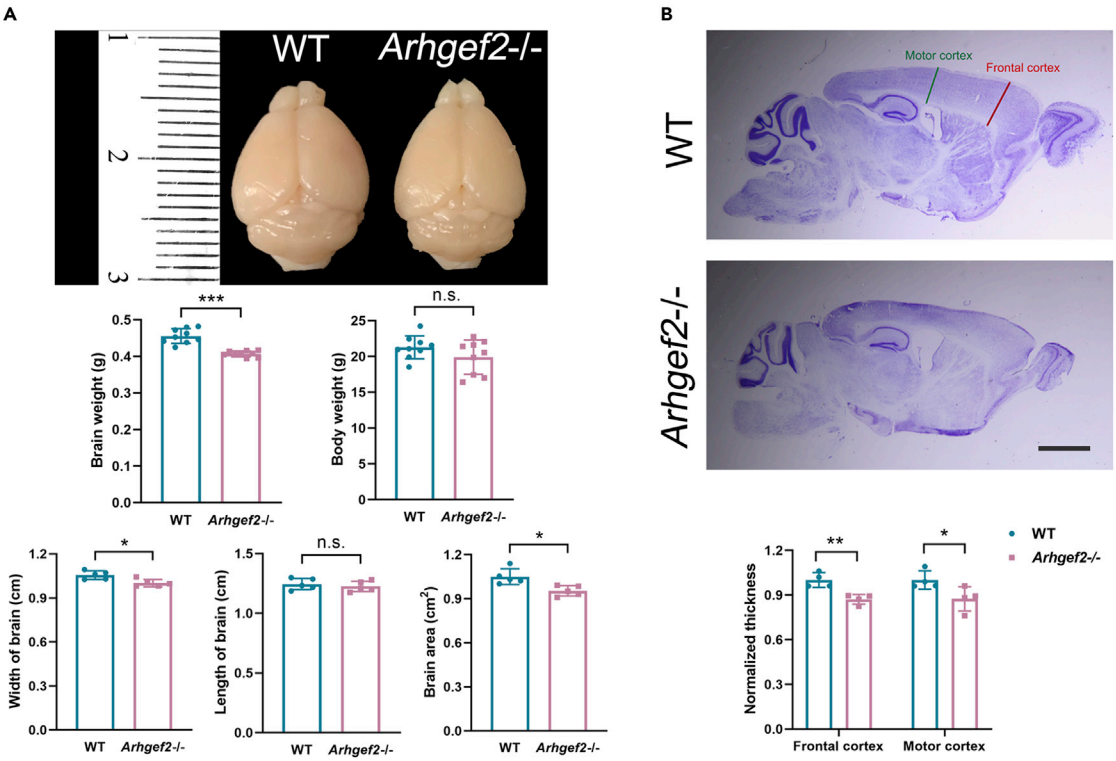

Figure 1. Microcephaly in *Arhgef2* knockout mouse model (postnatal 6 weeks)

(A) The brain weight and size were significantly decreased in *Arhgef2*−/− mice. n = 5–8 per genotype, ***p < 0.001, *p < 0.05, n.s.: no significant difference, unpaired t test.

(B) Nissl staining of sagittal brain sections. *Arhgef2*−/− mice showed a reduced thickness of frontal and motor cortex region compared with wild-type ones, 30 μm thick; scale bar, 2.5 mm, n = 4 per genotype, **p < 0.01, *p < 0.05, unpaired t test. Data are represented as mean ± S.D.

wild-type and *Arhgef2*−/− mice were observed, showing that m^{6}A peaks were abundant in the vicinity of start and stop codons (Figure S3A). Loss of *Arhgef2* resulted in the downregulation of 1,622 m^{6}A-containing mRNAs and upregulation of 1,073 m^{6}A-containing mRNAs. The cumulative distribution fraction of $\log_2$ (fold enrichment) demonstrated that m^{6}A methylation of mRNAs tended to be lower in *Arhgef2*−/− mice than that in wild-type mice (Figure S3B). Gene Ontology (GO) and KEGG pathway analysis of the 1,622 m^{6}A-tagged downregulated transcripts illustrated enrichment of genes related to cell communication, neurogenesis, neural differentiation, synapse organization, and cell cycle (Figures 3F and S3C). Interestingly, among 29 mRNAs that were both m^{6}A significantly downregulated and neural differentiation-related, we found two of the mRNAs (*Npdc1* and *Cend1*) strongly associated with cell cycle exit and terminal neural differentiation (Sansal et al., 2000; Politis et al., 2007) (Figures 3G and 3H). As *Arhgef2* downregulation keeps radial precursors cycling, and thereby inhibits neurogenesis (Ravindran et al., 2017), we thus speculated that *Npdc1* and *Cend1* played a vital role in this process. Compared with wild-type mice, protein level of *Npdc1* and *Cend1* apparently decreased in *Arhgef2*−/− mice, whereas mRNAs showed no significant change by qRT-PCR (Figures 4A–4D), suggesting the positive effect of m^{6}A modification on translation, nuclear export, or stability of both *Npdc1* and *Cend1*. Interestingly, in *Arhgef2*−/− mice, whereas polysome profiling demonstrated the significant decrease of *Npdc1* mRNA rather than *Cend1* mRNA (Figure 4E), nuclear RNA extraction showed an increased expression of *Cend1* mRNA, but not *Npdc1* mRNA (Figure 4F). These results indicated that Arhgef2 mediated the translation of *Npdc1* mRNA and nuclear export of *Cend1* mRNA.

Overexpression of Mettl14 rescued neurogenesis and morphology of neurons during neural differentiation

To characterize the impact of m^{6}A on neural differentiation, primary cells of *Arhgef2*−/− mice were transfected with HBLV-m-Mettl14/Zsgreen (Figure S6). The total m^{6}A level of primary neurons was significantly

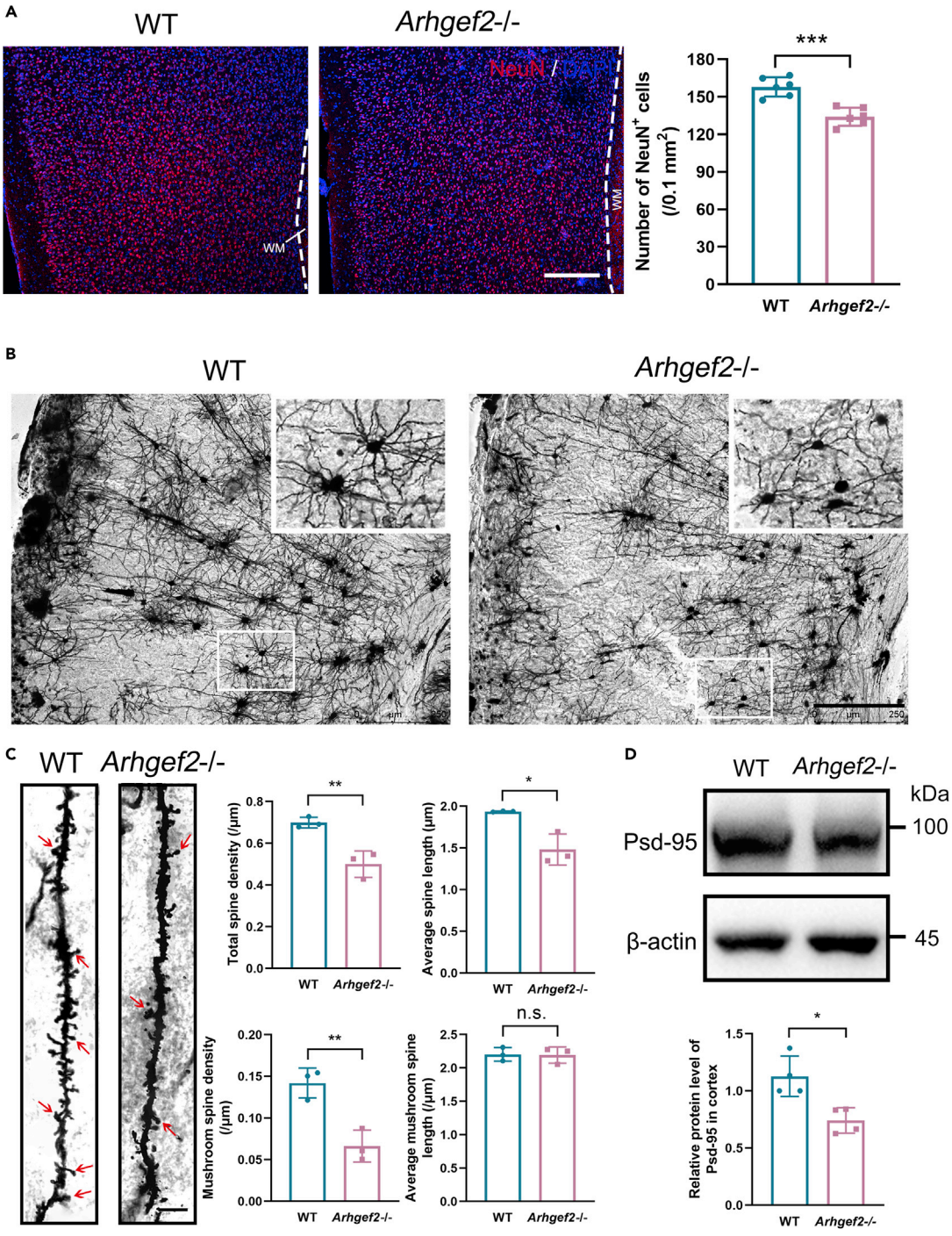

Figure 2. Abnormality of neural differentiation in *Arhgef2*-knockout mice model (postnatal 6 weeks)

(A) The number of NeuN$^+$ cells decreased significantly in *Arhgef2*−/− mice brain cortex compared with wild-type mice. Red: NeuN. Blue: DAPI. WM: white matter. Scale bar, 250 μm, n = 6, ***p < 0.001, unpaired t test.

(B) Representative images of Golgi staining. In *Arhgef2*−/− mice, morphology of neurites was abnormal. Scale bar, 250 μm.

(C) Total spines and mushroom spines significantly reduced in *Arhgef2*−/− mice compared with wild-type mice. The red arrow indicates mushroom spines. Scale bar, 5 μm. n = 3 per genotype, **p < 0.01, *p < 0.05, n.s.: no significant difference, unpaired t test.

(D) Compared with wild-type mice, expression of Psd-95 decreased significantly in *Arhgef2*−/− mice. n = 4 per genotype, *p < 0.05, unpaired t test. Data are represented as mean ± S.D.

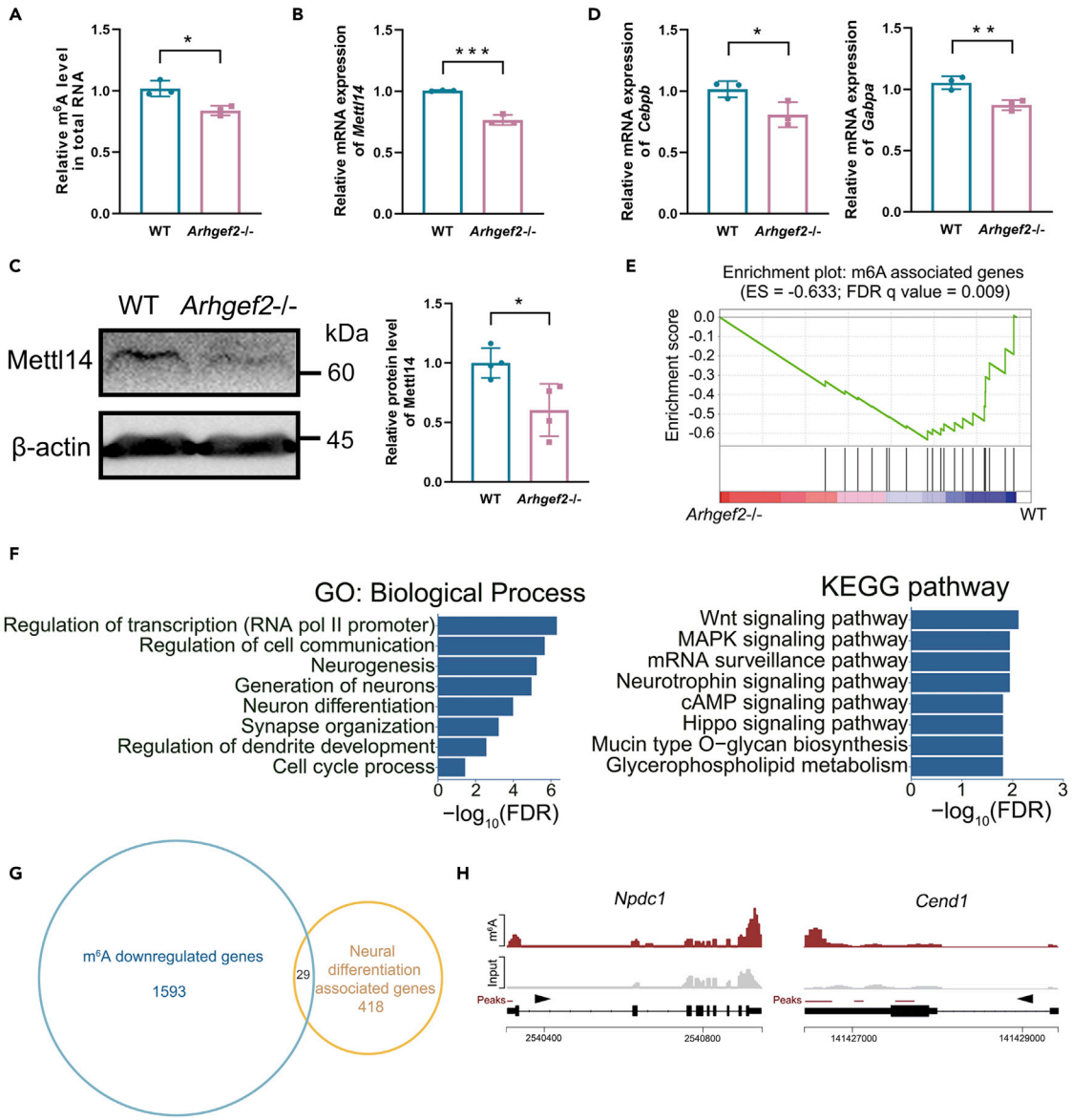

Figure 3. Loss of *Arhgef2* reduced m^{6}A level and led to the enrichment of m^{6}A-tagged mRNAs related to neural differentiation

(A) Total m^{6}A level of mouse brain cortex was determined by m^{6}A RNA Methylation Quantification Kit. n = 6, *p < 0.05, unpaired t test.

(B) The mRNA level of *Mettl14* examined by qRT-PCR was significantly decreased in *Arhgef2*−/− mice compared with wild-type mice. n = 3 per genotype, ***p < 0.001, unpaired t test.

(C) Representative western blot on brain cortex. Compared with wild-type mice, the protein expression of Mettl14 reduced in *Arhgef2*−/− mice. n = 4 per genotype, *p < 0.05.

(D) mRNAs of *Cebpb* and *Gabpa*, the translation factors of *Mettl14*, reduced significantly in *Arhgef2*−/− mice compared with wild-type mice. n = 3 per genotype (3 measurements for each sample), *p < 0.05, **p < 0.01, unpaired t test. Data are represented as mean ± SD.

(E) GSEA showed that the 21 m^{6}A-associated genes (*Mettl3, Mettl14, Mettl16, Wtap, Rbm15/15b, Kiaa1429, Fto, Alkbh5, Ythdc1/2, Ythdf1/2/3, eIF3, Abcf1, Fmr1, Igf2bp1/2/3, Cebpb, Gabpa*) were significantly enriched in the downregulated genes of *Arhgef2*−/− mice. n = 3 per genotype, q < 0.05, GSEA software v3.1.0.

(F) GO analysis of 1,622 downregulated m^{6}A-tagged genes revealed the enrichment for biological process terms related to transcription factors, cell communication, neurogenesis, synapse organization, and cell cycle. FDR, false discovery rate. Enrichment of KEGG pathway genes was also demonstrated.

(G) Venn diagram showing the overlap of m^{6}A downregulated mRNAs (p < 0.05) and neural differentiation-associated genes.

(H) Coverage plot of m^{6}A modification of *Npdc1* and *Cend1* mRNAs.

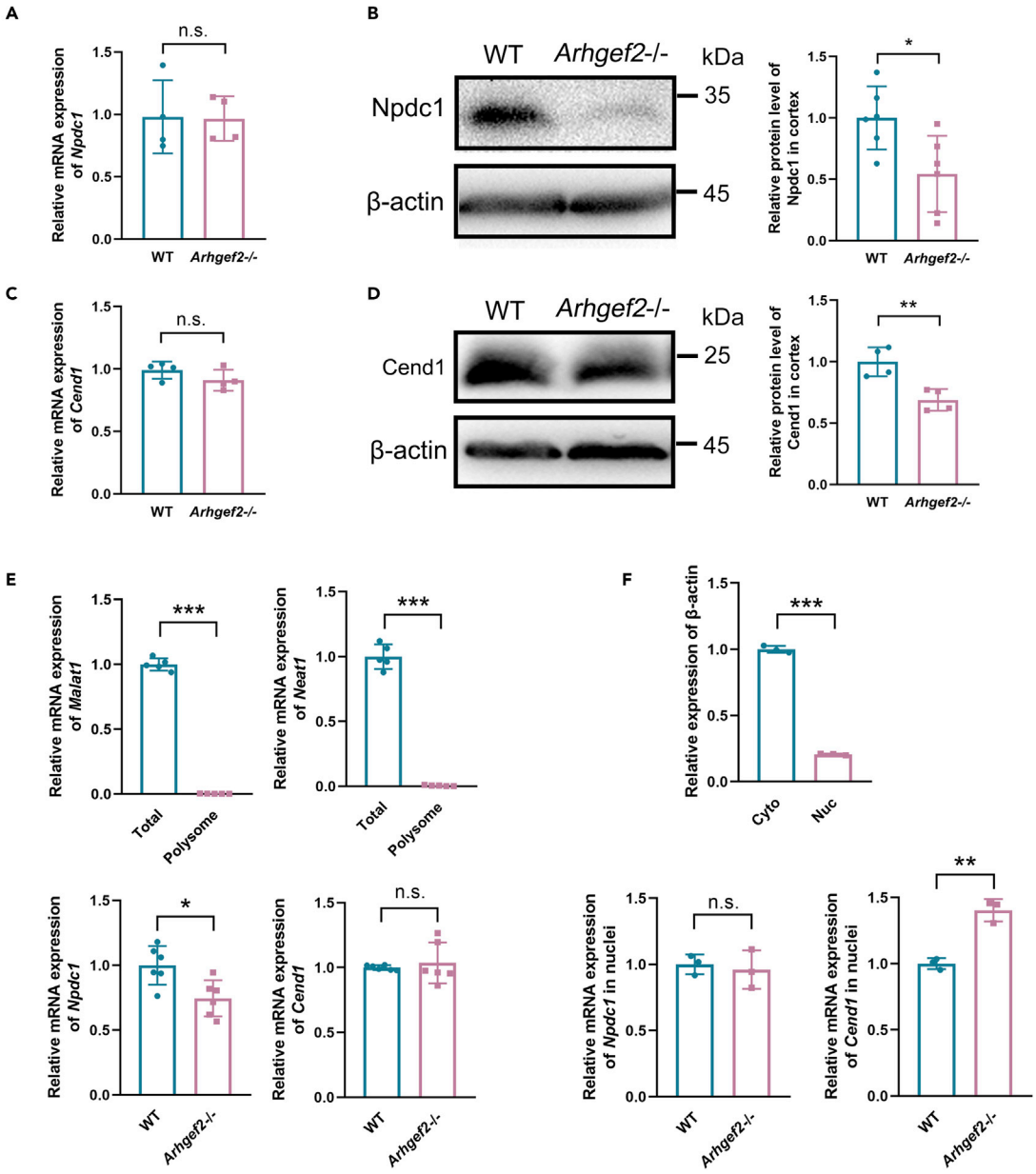

Figure 4. Loss of *Arhgef2* inhibited the translation of m^{6}A-modified *Npdc1* mRNA and nuclear export of m^{6}A-modified *Cend1* mRNA

(A–D) mRNA expression of *Npdc1* and *Cend1* showed no significant change determined by qRT-PCR. Protein levels of Npdc1 and Cend1 apparently decreased in *Arhgef2*−/− mice compared with wild-type ones. n.s.: no significant difference. n = 4–6 per genotype, *p < 0.05, **p < 0.01, unpaired t test.

(E) *Npdc1* mRNA expression in polysome fractions significantly reduced in *Arhgef2*−/− mice compared with wild-type ones, but *Cend1* mRNA showed no change. Poor expression of lncRNA (Malat1 and Neat1) in polysome fraction indicated the successful extraction of polysome fraction from other fractions. n.s.: no significant difference. *p < 0.05, ***p < 0.001, unpaired t test. Total: total RNA from brain tissue. Polysome: polysome fraction RNA.

(F) Compared with wild-type mice, the nuclear *Cend1* level, but not *Npdc1*, was significantly elevated in *Arhgef2*−/− mice. U1 was used as control gene in nuclei. Only low β-actin expression (~5-fold cytoplasm increase over nuclear) represented the successful separation of nuclear fractions. **p < 0.01, ***p < 0.001, unpaired t test. n.s.: no significant difference. Cyto: cytoplasm. Nuc: Nuclei. Data are represented as mean ± S.D.

increased with overexpression of Mettl14 (Figure S4A). RNA immunoprecipitation (RIP) demonstrated that the enrichment of m^{6}A-tagged *Npdc1* and *Cend1* mRNAs was significantly decreased in *Arhgef2*−/− RIP samples compared with wild-type RIP samples, which could be rescued after transfection with HBLV-m-Mettl14/Zsgreen (Figure S4B). Meanwhile, the distinct reduction of Npdc1 and Cend1 protein level in primary neurons from *Arhgef2*−/− mice also could be rescued by Mettl14 overexpression (Figure 5A). To

reveal whether NPCs remain in cell cycle and fail to enter neural differentiation pathway, we measured the size of cortical neurospheres at 72 h after transfection. A significantly increased size of spheres was examined in *Arhgef2*−/− mice compared with wild-type mice, and the phenotypic anomaly could be recovered by HBLV-m-Mettl14/Zsgreen (Figure 5B). In addition, we identified a fewer number of βIII-tubulin$^+$ cells (early neuron) and a larger proportion of βIII-tubulin$^-$Ki67$^+$ proliferating cells (precursors) in *Arhgef2*−/− mice than wild-type ones. Overexpression of Mettl14 was able to rescue this phenotype (Figure 5C). There was no significant variation in the proportion of phospho-histone H3 (pH3)-positive cells within 6 h of 5-ethynyl-2′-deoxyuridine (EdU) exposure (pH3$^+$EdU$^+$), suggesting that there was no defect in cell cycle to M phase by the loss of *Arhgef2* (Figure S5). We also found that overexpression of Mettl14 rescued impaired neurite outgrowth and post-synaptic formation (Psd-95 as marker) in *Arhgef2*−/− mice (Figures 6A-6C).

Overexpression of Npdc1 and Cend1 rescued neurogenesis and morphology of neurons during neural differentiation

To further determine the role of Npdc1 and Cend1 in this process, we designed to overexpress Npdc1 in Arhgef2−/− mice (Figure S6). The measurement of neuro-spheres size suggested that Npdc1 promoted cell cycle exit (Figure 7A). An increased number of βIII-tubulin$^+$ neurons and decreased number of βIII-tubulin$^-$Ki67$^+$ neurons were demonstrated in *Arhgef2*−/− mice transfected with HBLV-m-Npdc1/Zsgreen and HBLV-m-Cend1/Zsgreen, respectively (Figure 7B). Meanwhile, the abnormal morphology of neurite and expression of Psd-95 could also be, to some extent, rescued by overexpression of Npdc1 and Cend1 (Figures 8A and 8B).

DISCUSSION

m^{6}A is emerging as a vital factor regulating neural differentiation (Yoon et al., 2017; Meyer et al., 2012). Here, we illustrated that loss of *Arhgef2* reduced m^{6}A level of brain cortical neurons. Specifically, methylases Mettl14 showed the significant reduction, suggesting its critical role in neural differentiation regulated by *Arhgef2*. Interestingly, defective *Arhgef2* decreased m^{6}A modification of target mRNAs, and thereby regulated not only neurogenesis but also neurite outgrowth and synaptic formation during neural differentiation. The abnormal phenotypes could be rescued by Mettl14.

As *Arhgef2* down-regulation inhibits neurogenesis by keeping radial precursors cycling, and similar cellular phenotype is examined in *Mettl14* knockout mice (Ravindran et al., 2017; Yoon et al., 2017), it strongly led us to focus on two m^{6}A-modified target mRNAs (*Npdc1* and *Cend1*), which were associated with cell cycle exit and terminal neural differentiation. Several studies indicate that Npdc1 is a neuronal differentiation regulator, which interacts with E2F-1 and inhibits cell cycle progression by affecting the functions of E2F-1 (Sansal et al., 2000; Evrard et al., 2004). Npdc1 positively regulates neurite outgrowth and involves in NRF-1-regulated neurite outgrowth (Tong et al., 2013). *Cend1* (cell cycle exit and neuronal differentiation protein 1) coordinates cell cycle exit and differentiation of neuronal precursors (Politis et al., 2007). Deficiency of *Cend1* impairs differentiation of certain types of neurons, including Purkinje cells (Sergaki et al., 2010). Both *Npdc1* and *Cend1* are expressed in dividing NPCs and are increased when cells start to differentiate. Their expression is developmentally regulated and persists in adults along the neuronal lineage (Dupont et al., 1998; Gaitanou et al., 2019). *Arhgef2* deficiency decreased m^{6}A methylations of the *Npdc1* mRNA 5′ UTR and *Cend1* mRNA 3′ UTR, which thus inhibited the translation of *Npdc1* and nuclear export of *Cend1* mRNAs. As overexpression of Mettl14 in primary neurons from *Arhgef2*−/− mice rescued m^{6}A methylations of both target mRNAs, and thereby the protein level of Npdc1 and Cend1 was recovered near to wild-type ones, it suggested a significant impact of Mettl14-regulated m^{6}A methylations on the translation of target mRNAs. Overexpression of Npdc1 and Cend1 rescued the anomaly of neurogenesis, neurite outgrowth, and synaptic formation, indicating their persistent critical role during neuronal differentiation.

Synaptic formation is regarded as a vital process in postnatal brain, which is involved in precise communication between neurons and other cellular partners. Psd-95, the excitatory post-synaptic marker, has been implicated in synaptic development and plasticity, and its defects disturb learning and memory (Yoo et al., 2019; Zhang and Lisman, 2012; Zheng et al., 2011; Grant, 2012). In our work, loss of *Arhgef2* led to deficits in spine density and morphology and reduced expression of Psd-95 significantly. m^{6}A sequencing of mouse cortex also revealed enrichment of mRNAs related to cell communication and synapse organization. Deficits of synaptic formation thus were a pivotal factor to explain the intellectual disability caused by *Arhgef2* deficiency.

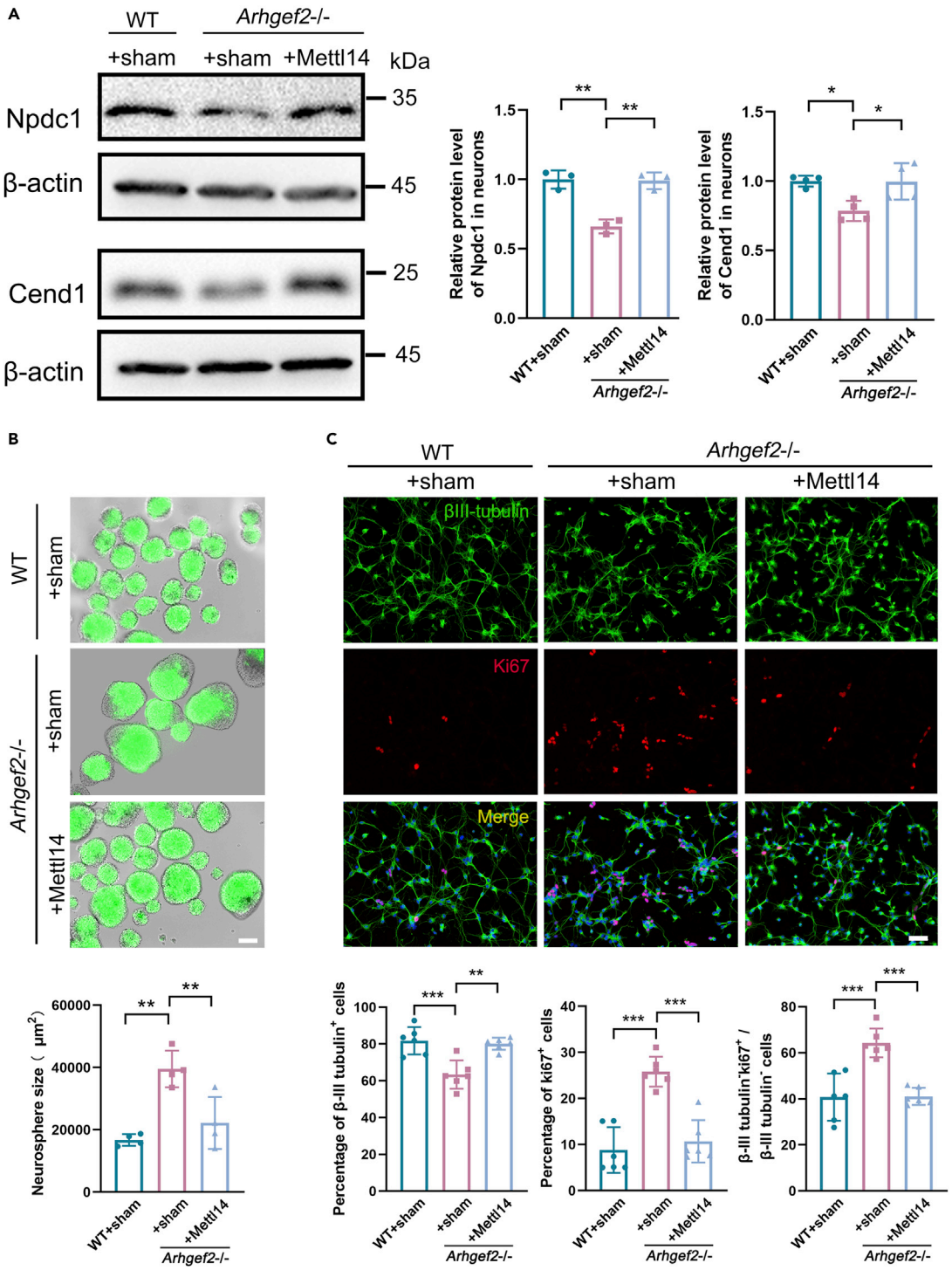

Figure 5. The anomaly of neurogenesis was rescued by overexpression of Mettl14 in primary NPCs from *Arhgef2*−/− mice (at E13.5)

(A) The protein expression of Npdc1 and Cend1 was examined by western blot. n = 3–4 per genotype, *p < 0.05, **p < 0.01, one-way ANOVA.

(B) The size of cortical neuro-spheres was measured at 72 h after transfection. A 2.3-fold increase of sphere size was noted by loss of *Arhgef2*, which could be recovered by HBLV-m-Mettl14-Zsgreen. Green: Zsgreen. Scale bar, 100 μm, n = 4 per genotype (3 measurements for each group), **p < 0.01, one-way ANOVA.

(C) Knockout of *Arhgef2* significantly decreased βIII-tubulin$^+$ cells (early neuron) and increased βIII-tubulin$^-$Ki67$^+$ proliferating cells (precursors), and the proportion could be rescued after Mettl14 overexpression. Cells were seeded at a density of 5 × 10^4/cm^2 and were observed at day 4 after transfection. βIII-tubulin, marker for early neuron, green; Ki67, marker for proliferating cells, red; DAPI, blue. Scale bar, 50 μm. n = 6 per genotype, **p < 0.01, ***p < 0.001, one-way ANOVA. Data are represented as mean ± SD.

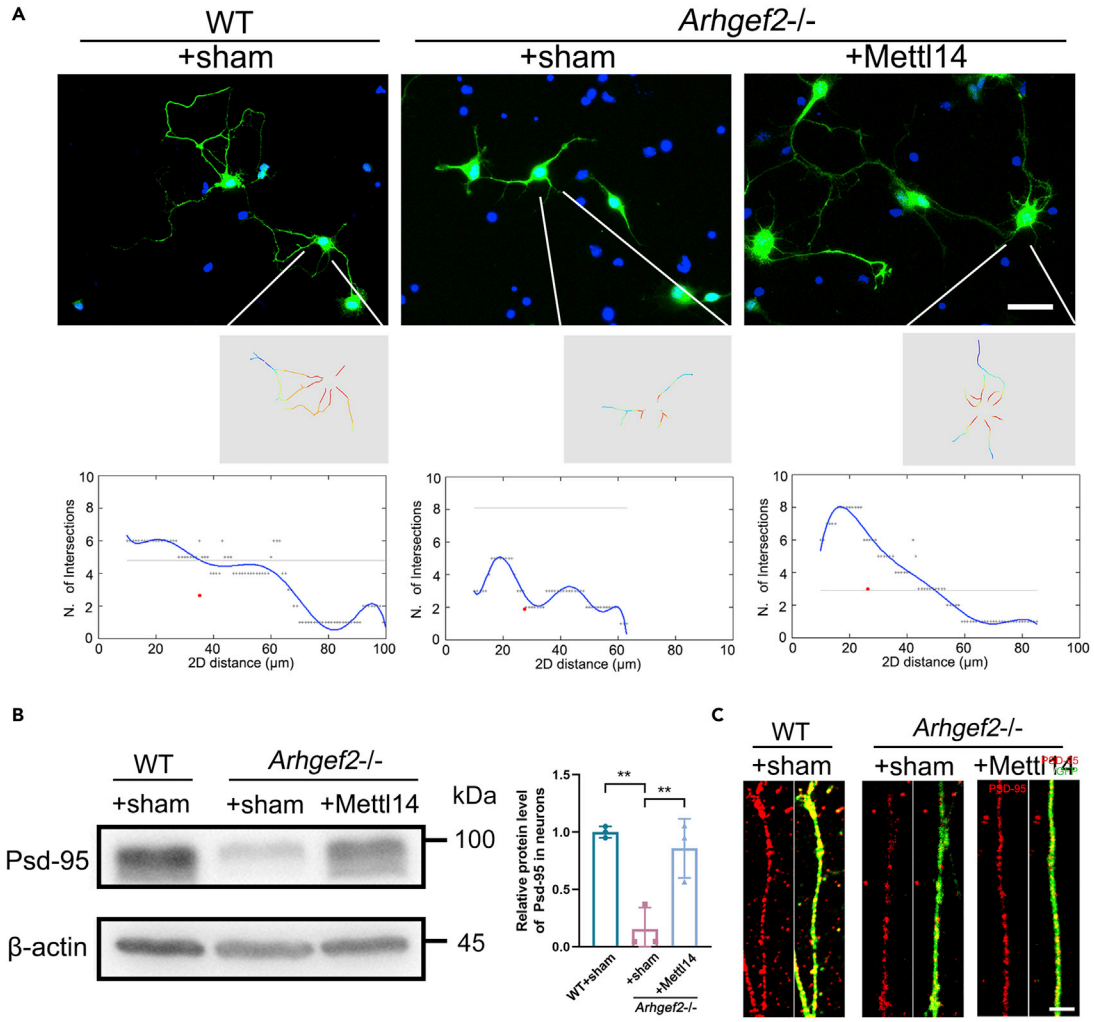

Figure 6. Overexpression of Mettl14 rescued the anomaly of neurite outgrowth and post-synaptic formation in primary neurons from *Arhgef2*−/− mice (at E13.5)

(A) The length of neurites and the number of branches of Zsgreen-positive cells was presented by using ImageJ combined with NeuronJ and Sholl Analysis plugin. *Arhgef2* deficiency reduced the longest length of neurites and branch number. Cells were seeded at a density of $2.5 \times 10^4/cm^2$ and were observed at day 3 after transfection. Scale bar, 25 μm.

(B) After transfection with HBLV-m-Mettl14-Zsgreen for 14 days, the expression of Psd-95 in primary matured neurons was measured by western blot analysis (left). Cells were seeded at a density of $1 \times 10^5/cm^2$ and were observed at day 14 after transfection. Data are presented as means ± SD from three independent experiments (right), n = 3 per genotype, $^{**}p < 0.01$, one-way ANOVA. Data are represented as mean ± SD.

(C) Immunostaining of Psd-95 in primary neurons. Psd-95 (marker for post-synapse, red), Zsgreen: green. Scale bar, 2.5 μm.

Arhgef2 catalyzes the replacement of GDP to GTP on RhoA (Birkenfeld et al., 2007). The GTP-bound form of RhoA causes Rho-associated kinase (ROCK) activation. Accumulating evidence point out that the RhoA/ROCK signaling participates in various neuronal functions, such as migration, dendrite development, and axonal extension (Fujita, 2014; Rico, 2004). In the last study, we reported that ARHGEF2-RhoA/ROCK pathway is essential for the migration and specification of precerebellar neurons. Specifically, the RhoA/ROCK/MLC pathway is most likely impaired in humans with the ARHGEF2 mutation (Ravindran et al., 2017). Several studies have indicated the role of RhoA/ROCK related to neural differentiation. NPCs with RhoA deficiency exhibit accelerated proliferation and reduction of cell cycle exit (Katayama et al., 2011). Activation of the RhoA/ROCK/JNK pathway could promote neuronal differentiation (Park et al., 2018).

However, whether ARHGEF2-RhoA/Rock pathway associated with m^6A modification during neural differentiation is still unclear. We thus examined the expression of Mettl14 in wild-type primary neurons with

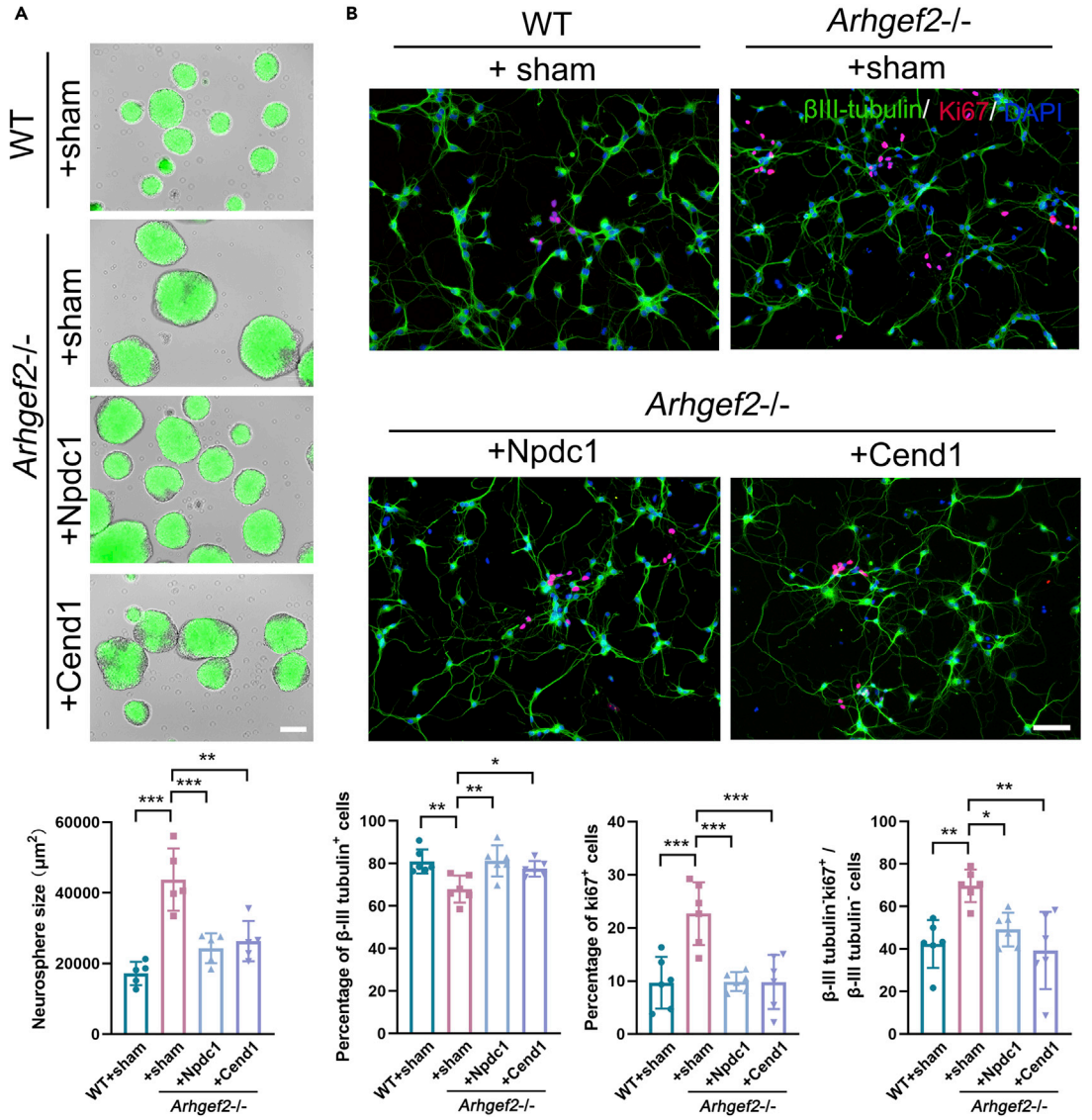

Figure 7. Overexpression of Npdc1 and Cend1 rescued the anomaly of neurogenesis in primary NPCs from *Arhgef2*−/− mice (at E13.5)

(A) Images of neuro-spheres showing a significant decrease size of spheres in *Arhgef2*-knockout NPCs after transfection with HBLV-m-Npdc1/Zsgreen and HBLV-m-Cend1/Zsgreen, respectively. Green: Zsgreen. Scale bar, 100 μm, n = 5 per genotype (2 measurements for each group), **p < 0.01, ***p < 0.001, one-way ANOVA.

(B) Both Npdc1 and Cend1 promoted the generation of βIII-tubulin$^+$ cells (early neuron) and decreased βIII-tubulin$^-$Ki67$^+$ proliferating cells (precursors). Cells were seeded at a density of 5 × 10^4/cm^2 and were observed at day 4 after transfection. βIII-tubulin, marker for early neuron, green; Ki67, marker for proliferating cells, red; DAPI, blue. Scale bar, 50 μm. n = 6 per genotype, *p < 0.05, **p < 0.01, ***p < 0.001, one-way ANOVA. Data are represented as mean ± SD.

treatment of Rock inhibitor Y27632. Surprisingly, mRNA and protein level of Mettl14 showed no significant change after treatment with Rock inhibitor, indicating that RhoA/Rock pathway maybe not implicated in Arhgef2/Mettl14-induced neuronal differentiation (Figure S7). Therefore, the exact pathway by which *Arhgef2* regulates *Mettl14* is worthy to be explored in the future work. Previous studies reported that Cebpb, Gabpa, Elf1, Cebpa, and Spi1 have binding sites within 5 kb upstream of the transcription start site of *Mettl14*. Among them, Gabpa and Elf1 showed a significant positive correlation, whereas *Spil* showed a significant negative correlation, with *Mettl14* (Weng et al., 2018). In *Arhgef2*−/− mice, *Cebpb* and *Gabpa* were significantly reduced compared with wild-type mice, suggesting *Arhgef2* was the most likely regulated expression of Mettl14 by them. This work elucidated a mechanism by which *Arhgef2* deficiency

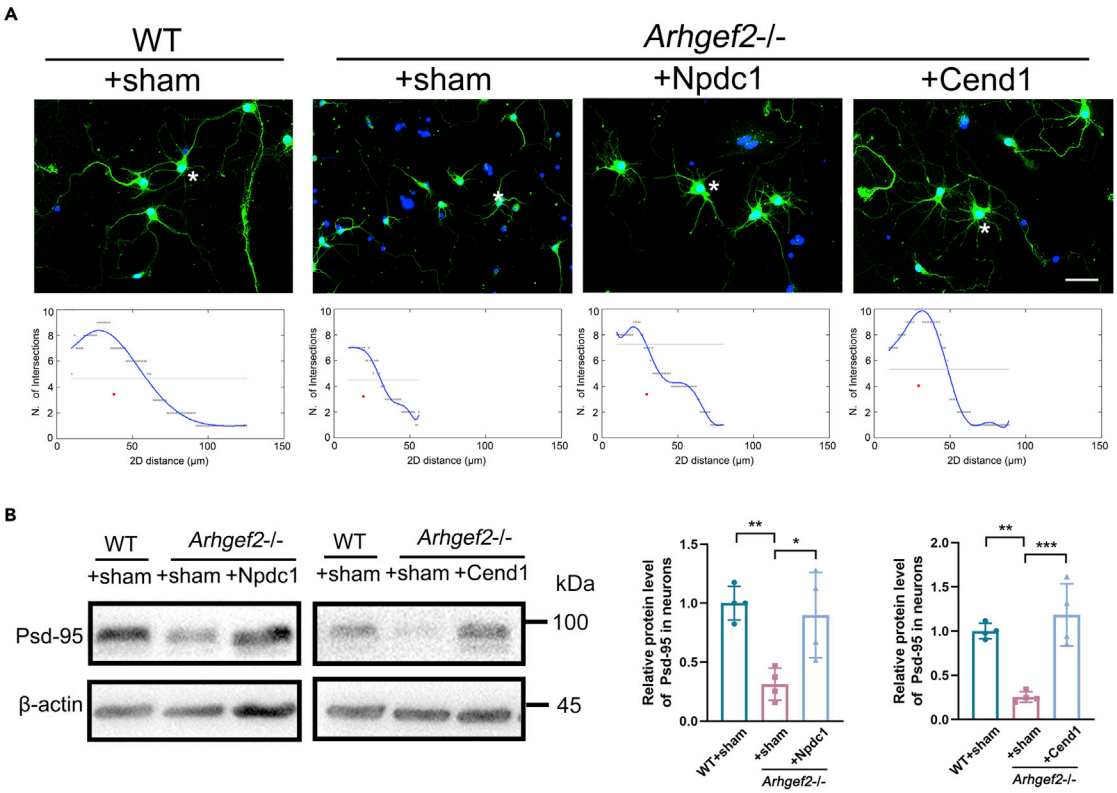

Figure 8. Overexpression of Npdc1 and Cend1 rescued the anomaly of neurite outgrowth in primary neurons from *Arhgef2*−/− mice (at E13.5)

(A) Measurement of the length of neurites and the number of branches of Zsgreen-positive cells. Cells were seeded at a density of 2.5 × 10^4/cm^2 and were observed at day 3 after transfection. Scale bar, 25 μm.

(B) After transfection with HBLV-m-Npdc1/Zsgreen and HBLV-m-Cend1/Zsgreen for 14 days, respectively, the expression of Psd-95 in primary matured neurons was measured by western blot analysis. Cells were seeded at a density of 1 × 10^5/cm^2 and were observed at day 14 after transfection. n = 4 per genotype, *p < 0.05, **p < 0.01, ***p < 0.001, one-way ANOVA. Data are represented as mean ± SD.

inhibited the translation of m^{6}A-modified *Npdc1* and nuclear export of *Cend1* mRNAs to impair neural differentiation. Intriguingly, it provided a considerable insight to think about the biological effects of the GEFs family on brain development associated with m^{6}A modification.

Limitations of the study

This study linked Arhgef2 and neurogenesis via m6A methylation of target mRNAs, including those of Npdc1/Cend1, which are involved in cell cycle exit and neuronal differentiation. However, according to our present study and others' literatures, it is still hard to know how Arhgef2 affects Mettl14 through Cebpb and Gabpa. Arhgef2, a member of the Rho guanine nucleotide exchange factor family, is crucial for controlling the Ras superfamily. Cebpb is an essential downstream mediator of Ras signaling, which could be phosphorylated by Ras expression. We thus speculate that Arhgef2 may regulate the expression of Cebpb via Ras signaling. As for Gabpa, it is hard for us to speculate based on literatures.

STAR★METHODS

Detailed methods are provided in the online version of this paper and include the following:

- KEY RESOURCES TABLE
- RESOURCE AVAILABILITY
  - Lead contact
  - Materials availability
  - Data and code availability

SUPPLEMENTAL INFORMATION

Supplemental information can be found online at https://doi.org/10.1016/j.isci.2021.102645.

ACKNOWLEDGMENTS

This work was supported by the National Natural Science Foundation of China (81671067, 81974163, and 82001121), the Major Medical Collaboration and Innovation Program of Guangzhou Science Technology and Innovation Commission (201604020020); the China Postdoctoral Science Foundation (2019M662852); and the Key-Area Research and Development Program of Guangdong Province (2019B020227001).

AUTHOR CONTRIBUTIONS

H.H. conceived and coordinated the project. P.Z. and N.L. oversaw the mice modeling with aids of S.Z., C.L., and L.L. P.Z. and Y.Q. designed and performed most of the experiments with aids of M.Y., S.Z., F.Q., H.L., Y.L., E.R., C.S., D.H., C.P., and N.L. X.F. was in charge of the genetic analysis and bioinformatics with aids of X.W. P.Z., and Y.Q. wrote the manuscript with aids of H.H., N.L., and A.M.K.

DECLARATION OF INTERESTS

The authors declare no competing interests.

Received: February 9, 2021
Revised: April 16, 2021
Accepted: May 20, 2021
Published: June 25, 2021

REFERENCES

Bailey, T.L., Boden, M., Buske, F.A., Frith, M., Grant, C.E., Clementi, L., Ren, J., Li, W.W., and Noble, W.S. (2009). MEME SUITE: tools for motif discovery and searching. Nucleic Acids Res. *37*, W202–W208. https://doi.org/10.1093/nar/gkp335.

Bakal, C.J., Finan, D., LaRose, J., Wells, C.D., Gish, G., Kulkarni, S., DeSepulveda, P., Wilde, A., and Rottapel, R. (2005). The Rho GTP exchange factor Lfc promotes spindle assembly in early mitosis. Proc. Natl. Acad. Sci. USA *102*, 9529–9534. https://doi.org/10.1073/pnas.0504190102.

Birkenfeld, J., Nalbant, P., Bohl, B.P., Pertz, O., Hahn, K.M., and Bokoch, G.M. (2007). GEF-H1 modulates localized RhoA activation during cytokinesis under the control of mitotic kinases. Dev. Cell *12*, 699–712. https://doi.org/10.1016/j.devcel.2007.03.014.

Chen, S., Zhou, Y.Q., Chen, Y., and Jia, G. (2018). fastp: an ultra-fast all-in-one FASTQ preprocessor. Bioinformatics *34*, i884–i890. https://doi.org/10.1093/bioinformatics/bty560.

Dupont, E., Sansal, I., Evarard, C., and Rouget, P. (1998). Developmental pattern of expression of NPDC-1 and its interaction with E2F-1 suggest a role in the control of proliferation and differentiation of neural cells. J. Neurosci. Res. *51*, 257–267. https://doi.org/10.1002/(SICI)1097-4547(19980115)51:2<257::AID-JNR14>3.0.CO;2-5.

Edens, B.M., Vissers, C., Su, J., Arumugam, S., Xu, Z., Shi, H., Miller, N., Rojas Ringeling, F., Ming, G.L., He, C., et al. (2019). FMRP modulates neural differentiation through m^6A-dependent mRNA nuclear export. Cell Rep *28*, 845–854.e5. https://doi.org/10.1016/j.celrep.2019.06.072.

Evrard, C., Caron, S., and Rouget, P. (2004). Functional analysis of the NPDC-1 gene. Gene *343*, 153–163. https://doi.org/10.1016/j.gene.2004.08.020.

Fujita, Y., and Yamashita, T. (2014). Axon growth inhibition by RhoA/ROCK in the central nervous system. Front. Neurosci. *8*, 338. https://doi.org/10.3389/fnins.2014.00338.

Gaitanou, M., Segklia, K., and Matsas, R. (2019). Cend1, a story with many tales: from regulation of cell cycle progression/exit of neural stem cells to brain structure and function. Stem Cells Int *2019*, 2054783. https://doi.org/10.1155/2019/2054783.

Grant, S.G. (2012). Synaptopathies: diseases of the synaptome. Curr. Opin. Neurobiol. *22*, 522–529. https://doi.org/10.1016/j.conb.2012.02.002.

Haussmann, I.U., Bodi, Z., Sanchez-Moran, E., Mongan, N.P., Archer, N., Fray, R.G., and Soller, M. (2016). m(6)A potentiates Sxl alternative pre-mRNA splicing for robust Drosophila sex determination. Nature *540*, 301–304. https://doi.org/10.1038/nature20577.

Heinz, S., Benner, C., Spann, N., Bertolino, E., Lin, Y.C., Laslo, P., Cheng, J.X., Murre, C., Singh, H., and Glass, C.K. (2010). Simple combinations of lineage-determining transcription factors prime cis-regulatory elements required for macrophage and B cell identities. Mol. Cell *38*, 576–589. https://doi.org/10.1016/j.molcel.2010.05.004.

Katayama, K., Melendez, J., Baumann, J.M., Leslie, J.R., Chauhan, B.K., Nemkul, N., Lang, R.A., Kuan, C.Y., Zheng, Y., and Yoshida, Y. (2011). Loss of RhoA in neural progenitor cells causes the disruption of adherens junctions and hyperproliferation. Proc. Natl. Acad. Sci. USA *108*, 7607–7612. https://doi.org/10.1073/pnas.1101347108.

Kim, D., Langmead, B., and Salzberg, S.L. (2015). HISAT: a fast spliced aligner with low memory requirements. Nat. Methods *12*, 357–360. https://doi.org/10.1038/nmeth.3317.

Koranda, J.L., Dore, L., Shi, H., Patel, M.J., Vaasjo, L.O., Rao, M.N., Chen, K., Lu, Z., Yi, Y., Chi, W., et al. (2018). Mettl14 is essential for Epitranscriptomic regulation of striatal function and learning. Neuron *99*, 283–292.e5. https://doi.org/10.1016/j.neuron.2018.06.007.

Krendel, M., Zenke, F.T., and Bokoch, G.M. (2002). Nucleotide exchange factor GEF-H1 mediates cross-talk between microtubules and the actin cytoskeleton. Nat. Cell. Biol. *4*, 294–301. https://doi.org/10.1038/ncb773.

Li, Q., Li, X., Tang, H., Jiang, B., Dou, Y., Gorospe, M., and Wang, W. (2017). NSUN2-mediated m5C methylation and METTL3/METTL14-mediated m6A methylation cooperatively enhance p21 translation. J. Cell. Biochem. *118*, 2587–2598. https://doi.org/10.1002/jcb.25957.

Meiri, D., Marshall, C.B., Greeve, M.A., Kim, B., Balan, M., Suarez, F., Bakal, C., Wu, C., Larose, J., Fine, N., et al. (2012). Mechanistic insight into the microtubule and actin cytoskeleton coupling through dynein-dependent RhoGEF inhibition. Mol. Cell *45*, 642–655. https://doi.org/10.1002/jcb.25957.

Meng, J., Lu, Z., Liu, H., Zhang, L., Zhang, S., Chen, Y., Rao, M.K., and Huang, Y. (2014). A protocol for RNA methylation differential analysis with MeRIP-Seq data and exomePeak R/Bioconductor package. Methods *69*, 274–281. https://doi.org/10.1016/j.ymeth.2014.06.008.

Merkurjev, D., Hong, W.T., Iida, K., Oomoto, I., Goldie, B.J., Yamaguti, H., Ohara, T., Kawaguchi, S.Y., Hirano, T., Martin, K.C., et al. (2018). Synaptic N6-methyladenosine (m6A) epitranscriptome reveals functional partitioning of localized transcripts. Nat. Neurosci. *21*, 1004–1014. https://doi.org/10.1016/j.ymeth.2014.06.008.

Meyer, K.D., and Jaffrey, S.R. (2014). The dynamic epitranscriptome: N6-methyladenosine and gene expression control. Nat. Rev. Mol. Cell Biol. *15*, 313–326. https://doi.org/10.1038/nrm3785.

Meyer, K.D., Saletore, Y., Zumbo, P., Elemento, O., Mason, C.E., and Jaffrey, S.R. (2012). Comprehensive analysis of mRNA methylation reveals enrichment in 30 UTRs and near stop codons. Cell *149*, 1635–1646. https://doi.org/10.1016/j.cell.2012.05.003.

Nalbant, P., Chang, Y.C., Birkenfeld, J., Chang, Z.F., and Bokoch, G.M. (2009). Guanine nucleotide exchange factor-H1 regulates cell migration via localized activation of RhoA at the leading edge. Mol. Biol. Cell *20*, 4070–4082. https://doi.org/10.1091/mbc.e09-01-0041.

Park, S.Y., Kang, M.J., and Han, J.S. (2018). Interleukin-1 beta promotes neuronal differentiation through the Wnt5a/RhoA/JNK pathway in cortical neural precursor cells. Mol. Brain *11*, 39. https://doi.org/10.1186/s13041-018-0383-6.

Pertea, M., Pertea, G.M., Antonescu, C.M., Chang, T.C., Mendell, J.T., and Salzberg, S.L. (2015). StringTie enables improved reconstruction of a transcriptome from RNA-seq reads. Nat. Biotechnol. *33*, 290–295. https://doi.org/10.1038/nbt.3122.

Politis, P.K., Makri, G., Thomaidou, D., Geissen, M., Rohrer, H., and Matsas, R. (2007). BM88/CEND1 coordinates cell cycle exit and differentiation of neuronal precursors. Proc. Natl. Acad. Sci. USA. *104*, 17861–17866. https://doi.org/10.1073/pnas.0610973104.

Ravindran, E., Hu, H., Yuzwa, S.A., Hernandez-Miranda, L.R., Kraemer, N., Ninnemann, O., Musante, L., Boltshauser, E., Schindler, D., Hübner, A., et al. (2017). Homozygous ARHGEF2 mutation causes intellectual disability and midbrain-hindbrain malformation. PLoS Genet *13*, e1006746. https://doi.org/10.1371/journal.pgen.1006746.

Ren, Y., Li, R., Zheng, Y., and Busch, H. (1998). Cloning and characterization of GEF-H1, a microtubule-associated guanine nucleotide exchange factor for Rac and Rho GTPases. J. Biol. Chem. *273*, 34954–34960. https://doi.org/10.1074/jbc.273.52.34954.

Rico, B., Beggs, H.E., Schahin-Reed, D., Kimes, N., Schmidt, A., and Reichardt, L.F. (2004). Control of axonal branching and synapse formation by focal adhesion kinase. Nat. Neurosci. *7*, 059–69. https://doi.org/10.1038/nn1317.

Roundtree, I.A., Luo, G.Z., Zhang, Z., Wang, X., Zhou, T., Cui, Y., Sha, J., Huang, X., Guerrero, L., Xie, P., et al. (2017). YTHDC1 mediates nuclear export of N6-methyladenosine methylated mRNAs. Elife *6*, e31311. https://doi.org/10.7554/eLife.31311.

Sansal, I., Dupont, E., Toru, D., Evrard, C., and Rouget, P. (2000). NPDC-1, a regulator of neural cell proliferation and differentiation, interacts with E2F-1, reduces its binding to DNA and modulates its transcriptional activity. Oncogene *19*, 5000–5009. https://doi.org/10.1038/sj.onc.1203843.

Sergaki, M.C., Guillemot, F., and Matsas, R. (2010). Impaired cerebellar development and deficits in motor coordination in mice lacking the neuronal protein BM88/Cend1. Mol. Cell Neurosci. *44*, 15–29. https://doi.org/10.1016/j.mcn.2010.01.011.

Shannon, P., Markiel, A., Ozier, O., Baliga, N.S., Wang, J.T., Ramage, D., Amin, N., Schwikowski, B., and Ideker, T. (2003). Cytoscape: a software environment for integrated models of biomolecular interaction networks. Genome Res. *13*, 2498–2504. https://doi.org/10.1101/gr.1239303.

Szklarczyk, D., Morris, J.H., Cook, H., Kuhn, M., Wyder, S., Simonovic, M., Santos, A., Doncheva, N.T., Roth, A., Bork, P., et al. (2017). The STRING database in 2017: quality-controlled protein–protein association networks, made broadly accessible. Nucleic Acids Res. *45*, D362–D368. https://doi.org/10.1093/nar/gkw937.

Tonami, K., Kurihara, Y., Arima, S., Nishiyama, K., Uchijima, Y., Asano, T., Sorimachi, H., and Kurihara, H. (2011). Calpain-6, a microtubule-stabilizing protein, regulates Rac1 activity and cell motility through interaction with GEF-H1. J. Cell. Sci. *124*, 1214–1223. https://doi.org/10.1242/jcs.072561.

Tong, C.W., Wang, J.L., Jiang, M.S., Hsu, C.H., Chang, W.T., and Huang, A.M. (2013). Novel genes that mediate nuclear respiratory factor 1-regualted neurite outgrowth in neuroblastoma IMR-32 cells. Gene *515*, 62–70. https://doi.org/10.1016/j.gene.2012.11.026.

Wang, X., Lu, Z., Gomez, A., Hon, G.C., Yue, Y., Han, D., Fu, Y., Parisien, M., Dai, Q., Jia, G., et al. (2014). N6-methyladenosine-dependent regulation of messenger RNA stability. Nature *505*, 117–120. https://doi.org/10.1038/nature12730.

Wang, Y., and Zhao, J.C. (2016). Update: mechanisms underlying N^6-methyladenosine modification of eukaryotic mRNA. Trends Genet. *32*, 763–773. https://doi.org/10.1016/j.tig.2016.09.006.

Weng, H., Huang, H., Wu, H., Qin, X., Zhao, B.S., Dong, L., Shi, H., Skibbe, J., Shen, C., Hu, C., et al. (2018). METTL14 inhibits hematopoietic stem/progenitor differentiation and promotes leukemogenesis via mRNA m6A modification. Cell Stem Cell *22*, 191–205.e9. https://doi.org/10.1016/j.stem.2017.11.016.

Yoo, K.S., Lee, K., Oh, J.Y., Lee, H., Park, H., Park, Y.S., and Kim, H.K. (2019). Postsynaptic density protein 95 (PSD-95) is transported by KIF5 to dendritic regions. Mol. Brain *12*, 97. https://doi.org/10.1186/s13041-019-0520-x.

Yu, G., Wang, L.G., and He, Q.Y. (2015). ChIPseeker: an R/Bioconductor package for ChIP peak annotation, comparison and visualization. Bioinformatics *31*, 2382–2383. https://doi.org/10.1093/bioinformatics/btv145.

Yoon, K.J., Ringeling, F.R., Vissers, C., Jacob, F., Pokrass, M., Jimenez-Cyrus, D., Su, Y., Kim, N.S., Zhu, Y., Zheng, L., et al. (2017). Temporal control of mammalian cortical neurogenesis by m(6)A methylation. Cell *171*, 877–889.e17. https://doi.org/10.1016/j.cell.2017.09.003.

Yoshizaki, H., Ohba, Y., Parrini, M.C., Dulyaninova, N.G., Bresnick, A.R., Mochizuki, N., and Matsuda, M. (2004). Cell type-specific regulation of RhoA activity during cytokinesis. J. Biol. Chem. *279*, 44756–44762. https://doi.org/10.1074/jbc.M402292200.

Zhang, P., and Lisman, J.E. (2012). Activity-dependent regulation of synaptic strength by PSD-95 in CA1 neurons. J. Neurophysiol. *107*, 1058–1066. https://doi.org/10.1152/jn.00526.2011.

Zheng, C.Y., Seabold, G.K., Horak, M., and Petralia, R.S. (2011). MAGUKs, synaptic development, and synaptic plasticity. Neuroscientist *17*, 493–512. https://doi.org/10.1177/1073858410386384.

Zhuang, Y.Y., Liu, H.J., Song, X., Ju, Y., and Peng, H. (2019). A linear regression predictor for identifying N(6)-Methyladenosine sites using frequent gapped K-mer pattern. Mol. Ther. Nucleic Acids *18*, 673–680. https://doi.org/10.1016/j.omtn.2019.10.001.

STAR★METHODS

KEY RESOURCES TABLE

REAGENT or RESOURCE	SOURCE	IDENTIFIER
Antibodies		
Mouse monoclonal anti-m^{6}A	Millipore	Cat no: MABE1006
Mouse monoclonal anti-NeuN	Millipore	Cat no: MAB377B; RRID: AB_177621
Mouse monoclonal anti-β-III tubulin	Millipore	Cat no: MAB1637; RRID: AB_2210524
Rabbit polyclonal anti-Ki67	Abcam	Cat no: 9129; RRID: AB_2687446
Rabbit polyclonal anti-Psd-95	Cell Signaling Technology	Cat no: 3450;RRID: AB_2292883
Mouse monoclonal anti-Synaptophysin	Abcam	Cat no: ab8049; RRID: AB_2198854
Rabbit polyclonal anti-Mettl14	Cell Signaling Technology	Cat no:51104S; RRID: AB_2799383
Rabbit polyclonal anti-Npdc1	Affinity	Cat no: DF4225; RRID: AB_2836576
Rabbit monoclonal anti-Cend1	Abcam	Cat no: ab113076; RRID: AB_10860676
Rabbit polyclonal anti-Phospho-Histone H3 (Ser10)	Cell Signaling Technology	Cat no:9701; RRID: AB_331535
Rabbit monoclonal anti-β-actin(D6A8)	Cell Signaling Technology	Cat no: 8457; RRID: AB_10950489
Goat anti-Rabbit IgG (H+L) Highly Cross-Adsorbed Secondary Antibody, Alexa Fluor 568	Thermo Fisher Scientific	Cat no: A-11036; RRID: AB_10563566
Goat anti-Mouse IgG (H+L) Highly Cross-Adsorbed Secondary Antibody, Alexa Fluor 647	Thermo Fisher Scientific	Cat no: A-21236; RRID: AB_2535805
Anti-rabbit IgG, HRP-linked Antibody	Cell Signaling Technology	Cat no: 7074; RRID: AB_2099233
Anti-mouse IgG, HRP-linked Antibody	Cell Signaling Technology	Cat no: 7076; RRID: AB_330924
Deposited data		
m^{6}A-sequencing data	This paper	PRJNA730635
Critical commercial assays		
FD Rapid GolgiStain^{TM} kit	Neuro Technologies	Cat no: PK401
m^{6}A RNA Methylation Quantification Kit (Colorimetric)	Abcam	Cat no: ab185912
Imprint RNA Immunoprecipitation (RIP) Kit	Sigma-Aldrich	Cat no: RIP-12RXN
Click-iT EdU Imaging Kits	Thermo Fisher Scientific	Cat no: C10339
Experimental models: Organisms/strains		
Arhgef2 knockout mice	Shanghai Biomodel Organism Science & Technology Development	N/A
Oligonucleotides		
β-actin: (F) 5′-GGCTGTATTCCCCTCCATCG-3′ (R) 5′-CCAGTTGGTAACAATGCCATGT-3′	This paper	N/A

(*Continued on next page*)

Continued

REAGENT or RESOURCE	SOURCE	IDENTIFIER
Arhgef2: (F) 5′-ATCTCCGTCTCCGGCATGA-3′ (R) 5′-CAGGGTGTCTTTACAGCGGTT-3′	This paper	N/A
Npdc1: (F) 5′-CTTCAACACCACGAATCTCGC-3′ (R) 5′-CCTTTGGAGGTTCCTTATGCC-3′	This paper	N/A
Cend1: (F) 5′-ACCAGCCAAGGCAGATCCT-3′ (R) 5′-GGTCAAGTTCTCACAAGGCCA-3′	This paper	N/A
Mettl14: (F) 5′-TCTGAGAGTGCGGATAGCATTG-3′ (R) 5′-GAGCAGATGTATCATAGGAAGCC-3′	This paper	N/A
Mettl3: (F) 5′-CTGGGCACTTGGATTTAAGGAA-3′ (R) 5′-TGAGAGGTGGTGTAGCAACTT-3′	This paper	N/A
Wtap: (F) 5′-ATGGCACGGGATGAGTTAATTC-3′ (R) 5′-TTCCCTTAAACCAGTCACATCG-3′	This paper	N/A
Fto: (F) 5′-CCGTCCTGCGATGATGAAGT-3′ (R) 5′-CCCATGCCGAAATAGGGCTC-3′	This paper	N/A
Alkbh5: (F) 5′-TTGCCACCCAGCTATGCTTC-3′ (R) 5′-CAGACCGCCGGTTTTCTTCTT-3′	This paper	N/A
Gabpa: (F) 5′-AGCGCATCTCGTTGAAGAAG-3′ (R) 5′-TCCTGCTCTTTTCTGTAGCCT-3′	This paper	N/A
Cebpb: (F) 5′-CAAGATGCGCAACCTGGAGA-3′ (R) 5′-GACAGCTGCTCCACCTTCTT-3′	This paper	N/A
Cebpa: (F) 5′-CAAGAACAGCAACGAGTACCG-3′ (R) 5′-GTCACTGGTCAACTCCAGCAC-3′	This paper	N/A
Elf1: (F) 5′-TGTCCAACAGAACGACCTAGT-3′ (R) 5′-CACACAAGCTAGACCAGCATAA-3′	This paper	N/A
Spi1: (F) 5′-ATGTTACAGGCGTGCAAAATGG-3′ (R) 5′-TGATCGCTATGGCTTTCTCCA-3′	This paper	N/A
Malat1: (F)5′-CATGGCGGAATTGCTGGTA-3′ (R)5′-CGTGCCAACAGCATAGCAGTA-3′	This paper	N/A
Neat1: (F)5′-TGGCCCCTTTTGTTCATTAGC-3′ (R)5′-TGGAAGGCCATTGTTTCAGG-3′	This paper	N/A
U1: (F) 5′-GATACCATGATCACGAAGGTGGTT-3′ (R) 5′-CACAAATTATGCAGTCGAGTTTCC-3′	This paper	N/A
Recombinant DNA		
HBLV-m-mettl14-3xflag-Zsgreen-PURO	Hanbio	N/A
HBLV-m-Npdc1-3xflag-Zsgreen-PURO	Hanbio	N/A
HBLV-m-Cend1-3xflag-Zsgreen-PURO	Hanbio	N/A
Software and algorithms		
Prism 7	GraphPad	SCR_002798; https://www.graphpad.com
ImageJ	Wayne Rasband National Institutes of Health	https://imagej.nih.gov/ij/
Fastp	Chen et al., 2018	https://github.com/OpenGene/fastp
IGV	Meng et al., 2014	http://www.igv.org

RESOURCE AVAILABILITY

Lead contact

Further information and requests for resources and reagents should be directed to and will be fulfilled by the Lead Contact, Hao Hu (huh@cougarlab.org).

Materials availability

This study did not generate new unique reagents.

Data and code availability

Sequencing data have been deposited with the Sequence Read Archive (SRA) under BioProject :PRJNA730635(https://www.ncbi.nlm.nih.gov/bioproject/PRJNA730635).

EXPERIMENTAL MODEL AND SUBJECT DETAILS

Mice model establishment

All mice experiments in this work were approved by the institutional animal care and use committee in the Guangzhou Medical University (registration No. 2019-436, 2019-694). *Arhgef2* knockout mice were created using *CRISPR/Cas9*-mediated genome engineering. Exon 2 was selected as the target site, and gRNA was designed as following sequences: gRNA1: 5′-ACCTACCTGACCCCGGCGACTGG-3′; gRNA2: 5′-TATTG GAATGTGGCGTAAGCTGG-3′.

The zygotes co-injected with Cas9 mRNA and gRNA were cultured in medium until the two-cell stage, and then were transferred into the oviducts of pseudopregnant ICR females. After being identified by genomic PCR and Sanger sequencing, the mutant F0 were bred with C57BL/6J males to yield heterozygous *Arhgef2* mice. Subsequent breeding of the heterozygous *Arhgef2* mice generated offspring with wild-type and knockout littermates for experiments. For animal experiments, *Arhgef2* knockout male and female mice (sex balance) at age of 6-8 weeks were used. For primary cell culture, *Arhgef2* heterozygous pregnant mice were used.

Cell culture

Primary mouse NPCs were isolated from *Arhgef2* wild-type and knockout mice embryonic cortices at E13.5 and cultured in Neurobasal medium (Gibco, CA, USA) containing 2% B27 (v/v, Gibco), 0.25% Glutamax, and 25 μM glutamate. Cells were seeded on dishes precoated with poly-D-lysine. To measure neuro-spheres, NPCs were cultured in ultra-low attachment plates and the size pf spheres was analyzed by Image J. The experiments of neurogenesis were performed on density-matched NPCs cultures within the first 4 days, while the experiments related to synaptic formation were conducted in well-matured neurons at day 14. For the overexpression of Mettl14 or Npdc1, transfection of HBLV-m-Mettl14/Zsgreen and HBLV-m-Npdc1/Zsgreen (at MOI 10) (Hanbio Biotechnology, Shanghai, China) respectively to *Arhgef2*-knockout primary cells was performed. HBLV-Zsgreen was transfected to wild-type and *Arhgef2* -knockout cells as control.

METHOD DETAILS

Tissue preparation

Mice at 6 weeks of age were anaesthetized with 50 mg/kg sodium pentobarbital. After perfused with 0.9% NaCl and 4% PFA, brains were harvested and fixed in 4% PFA overnight, followed with dehydration by 15% and 30% sucrose. Sagittal brain sections (30 μm thick) were prepared using freezing microtome (CM3050S, Leica, Germany).

Nissl staining

Brain sections were treated with 75% ethanol for 30 s, dH_2O for 30 s and cresyl violet for 2 min. After dehydration with gradient ethanol (75%, 95%, 100%), sections were incubated with xylene and mounted using neutral resins. The images were taken under microscope.

Immunostaining

To determine the number of matured neurons in brain cortex, sections were permeabilized with 0.3% Triton X-100 and blocked with goat serum for 1 h at room temperature, followed by incubation with mouse anti-NeuN antibody at 4°C overnight. After washing, HRP-conjugated anti-mouse IgG secondary antibody was applied to the sections for 1 h at room temperature. Nuclei were stained using 4,6-diamidino-2-phenylindole (DAPI, Thermo Fisher Scientific).

To examine the neurogenesis of NPCs, cells were immersed in 4% PFA for fixation, 0.3% Triton X-100 for permeabilization, and then blocking. Cells were incubated with mouse anti-β-III tubulin antibody and

rabbit anti-ki67 antibody overnight, followed by secondary antibodies. To observe the synaptic formation, Zsgreen-positive cells were co-staining with Psd-95 as above. Immunostaining of pH3 in primary cells exposed to EdU was also performed as above. Data were obtained from at least three independent experiments and analyzed by ImageJ software.

Golgi staining

Brain tissue prepared for Golgi staining was performed by using FD Rapid GolgiStain™ kit. According to manufacturer's instruction, tissue was immersed in Solution A/B at room temperature for at least 24 h, followed by Solution C. All procedures should be protected from light. Samples embedded in OCT compound were then sectioned coronally (30 μm thick). For staining procedure, sections were placed in Solution D/E for 10 min. After washing, sections were dehydrated in 50%, 75%, and 95% ethanol, followed by 100% ethanol 4 times for 4 min each rinse. Sections then were cleared by xylene and mounted. The confocal imaging was achieved using a TCS-SP8 LSM confocal imaging system (Leica, Wetzlar, Germany).

Quantification of the m^{6}A

The m^{6}A level of brain cortex was measured using m^{6}A RNA Methylation Quantification Kit (Colorimetric). In brief, total RNA of brain cortex was isolated using TRIZOL reagent (Invitrogen, Thermo Fisher Scientific, USA). 100 -300 ng total RNA per reaction was added into the wells filled with 80 μl Binding Solution. After incubation at 37°C for 90 min, wells were washed with 1X Wash Buffer. m^{6}A RNA was then captured using Diluted Capture Antibody, following by Diluted Detection Antibody and Diluted Enhancer Solution. Developer Solution was added to each well and incubated for 1-10 min away from light. Signal was detected on a microplate reader at 450 nm.

Quantitative real-time PCR (qPCR)

Total RNA was extracted from the mice brain tissues using TRIZOL reagent (Invitrogen, Thermo Fisher Scientific, MA, USA), and first-strand cDNA was synthesized with PrimeScript RT reagent (Takara-Clonetech, Shiga, Japan). qRT-PCR was performed using SYBR Premix Ex TaqII (Takara-Clonetech) and analyzed with Fast Real Time System 7500 (Applied Biosystems). Expression levels of each target gene were measured relative to β-actin as internal control. The following sequences of primers were exhibited in Table (Table S1). The experiments were repeated at least three times, each time with consistent results.

m^{6}A-sequencing

Total RNA was isolated from the cortex samples of the WT and KO mice and purified using TRIzol reagent following the manufacturer's procedure. The RNA integrity was determined and confirmed using Bioanalyzer 2100 (Agilent, CA, USA) with RIN number >7.0 and electrophoresis with denaturing agarose gel, respectively. Using Dynabeads Oligo (dT) 25-61005 (Thermo Fisher, CA, USA), Poly (A) RNA was purified from 50 μg total RNA under two rounds of purification. Under 86°C, the poly (A) RNA was fragmented into small pieces using Magnesium RNA Fragmentation Module (NEB, cat. e6150, USA) for 7 min. m^{6}A pull-down was performed using m^{6}A-specific antibody (No. 202003, Synaptic Systems, Germany) in IP buffer (50 mM Tris-HCl, 750 mM NaCl and 0.5% Igepal CA-630) for 2 h at 4°C. Next, the IP RNA was reverse-transcribed to cDNA, followed by synthesis of U-labeled second-stranded DNAs with E. coli DNA polymerase I (NEB, cat.m0209, USA), RNase H (NEB, cat.m0297, USA) and dUTP Solution (Thermo Fisher, cat. R0133, USA).

An A-base was then added to the blunt ends of each strand, which was prepared for ligation to the indexed adapters. Single- or dual-index adapters were ligated to the fragments; size selection was performed with AMPureXP beads. After the heat-labile UDG enzyme (NEB, cat.m0280, USA) treatment, the ligated products were amplified with PCR. The average insert size for the final cDNA library was 300 ± 50 bp. The 2 ×150 bp paired-end sequencing (PE150) was performed on an illumina Novaseq™ 6000 (LC-Bio Technology CO., Ltd., Hangzhou, China).

Bioinformatic analyses of m^{6}A-seq

The reads containing adaptor contamination, low quality bases and undetermined bases were removed using the fastp software (Chen et al., 2018) with default parameter. Sequence quality of IP and Input samples was verified by Fastp. The reads were then mapped to the reference genome Mus musculus (Version: v99) using HISAT2 (Kim et al., 2015). The m^{6}A peaks with bed or bigwig format that can be adapted for

visualization on the IGV software (http://www.igv.org) were identified by the R package exomePeak (Meng et al., 2014). MEME (Bailey et al., 2009) and HOMER (Heinz et al., 2010) were used for de novo and known motif finding, followed by localization of the motif with respect to peak summit. Called peaks were annotated using R package ChIPseeker (Yu et al., 2015). The expression level for all mRNAs from input libraries was determined using StringTie (Pertea et al., 2015) by calculating FPKM (total exon fragments /mapped reads (millions) × exon length (kB)). Gene ontology analysis was performed on the 1622 m^6A downregulated genes using GO enrichment analysis tool of Omicshare. KEGG pathway analysis was also performed on the 1622 m^6A downregulated genes using pathway enrichment analysis tool of Omicshare. GO terms and KEGG pathways with FDR corrected $p < 0.05$ was considered significant. Protein-protein interaction network was obtained from the STRING database (Szklarczyk et al., 2017). The interaction network model was generated using Cytoscape 3.6.1 (Shannon et al., 2003). The lastest gene list was downloaded from the BioMart database (https://www.ensembl.org/biomart/martview/) where 447 neural differentiation associated genes were identified according to their functional annotation and related GO terms.

Neurite outgrowth analysis

Neurite outgrowth of Zsgreen-positive cells was measured using Image J combined with Neuron J and Sholl Analysis plugin. A vertical line from the soma to the tip of the longest branch was drawn to defined as the length of neurite. the number of branches was examined by counting the intersections of neurites and concentric circles. The radius interval between circles was 10 μm per step, ranging from 10 μm to the tips of the longest branch.

EdU staining

Primary cells were labeled with 10 μM EdU solution and incubated for 4 h at 37°C and then fixed with 4% PFA. After permeabilization with 0.5% TritonX-100, cells were treated with Click-iT EdU Imaging Kits according to manufacturer's protocol.

RNA immunoprecipitation (RIP)

After transfection of lentivirus for 3 days, m6A modification on Npdc1 and Cend1 mRNA was detected using Imprint RNA Immunoprecipitation (RIP) Kit. In brief, cells (1-2 X 10^6 each reaction) were collected in mild lysis buffer supplemented with protease inhibitor cocktail, 1 M DTT and 40 U/μl ribonuclease inhibitor. After incubation on ice for 15 min, the lysis reactions were centrifuged for 10 min at 16,000 *g* at 4°C, and supernatant was collected. 10% of RIP lysate supernatant per reaction was labelled as Input. Each reaction was then incubated with 2 μg of anti-m^6A antibody-prebinding protein A magnetic beads on a rotator overnight. 2 μg of IgG antibody was used for negative control. m^6A-tagged mRNA was eluted by IP buffer and purified using TRIZOL reagent. SYBR-green based qRT-PCR was performed as described above.

Western blot

Protein was extracted using 2% SDS containing protease inhibitor cocktail and phosphatase inhibitor (Cell Signaling Technology, MA, USA). Samples were separated with 12.5% SDS-PAGE and transferred to PVDF membranes (Millipore, MA, USA). The membranes were blocked in 5% skim milk for 1 h at room temperature and then incubated overnight at 4°C with the following primary antibodies: rabbit anti-Npdc1 antibody, rabbit anti-Cend1 antibody, rabbit anti-Mettl14 antibody, rabbit anti-Psd-95 antibody, and mouse anti-Synaptophysin antibody, respectively. After washing with TBST, the membranes were incubated with secondary antibodies for 1 h at room temperature. Blots were visualized by ChemiDocTM MP system (Bio-Rad, USA) and then quantified via ImageJ software.

Polysome profiling

10%~45% sucrose density gradients were prepared using sucrose gradient buffer (10 mM HEPES-KOH, 5 mM MgCl2, 150 mM KCl, 200 U/ml RNase inhibitor, 1x protease inhibitor cocktail, 100 μg/ml cycloheximide). Brain tissue was grinded in a liquid nitrogen-proof container to obtain powder. The powder was collected in a modified lysis buffer (10 mM HEPES-KOH, 5 mM MgCl2, 150 mM KCl, 0.5 mM DTT, 100 U/ml RNase inhibitor, 1x protease inhibitor cocktail, 100 μg/ml cycloheximide, 0.5% NP-40, 0.05% Triton-X100) and further homogenized using electric grinding rod. The homogenate was centrifuged at 20000 rcf for 10 min at 4°C or reserved for total RNA isolation. The supernatant was layered onto sucrose gradient and centrifuged in a SW-40Ti rotor at 36,000 rpm for 2.5 h at 4°C and then analyzed using Gradient Fractionator (Biocomp). Polysome fraction was collected and RNA was extracted with TRIzol LS Reagent

(Invitrogen, MA, USA) according to manufacturer's instructions. qRT-PCR was performed as described above. LncRNA (*Malat1* and *Neat1*) was used as quality control of polysome fraction.

Nuclear RNA extraction

Homogenization of mice brain tissue with liquid nitrogen grinding, and nuclear fractions were prepared using NE-PER Nuclear and Cytoplasmic Extraction Kit (Thermo Fisher Scientific) according to the manufacturer's protocol. 100U/ml of RNase inhibitor (Ambon/Fisher) was added to the CERI reagent to prevent RNA degradation. After separation from the cytoplasmic fraction, the nuclear fraction was washed twice with ice PBS (prepared in RNase-free water), and resuspended in an appropriate volume of TRIzol reagent (Invitrogen). RNA was purified using the TRIzol reagent manufacturer's protocol. The efficiency of separation was determined by measuring nuclear and cytoplasmic RNA fractions by qRT-PCR for the ratio of β-actin expression in nuclei and cytoplasm. Only nuclear RNA preparations with low β-actin expression (~5-fold cytoplasm increase over nuclear) were used for analysis. To compare the expression of *Npdc1* and *Cend1* mRNA in nuclei, U1 was used as control gene.

QUANTIFICATION AND STATISTICAL ANALYSIS

Statistical analysis was performed using GraphPad Prism8 software. All graphs present mean ± S.D. Statistical comparisons of the data were carried out by student's t-test and One-way ANOVA. $P<0.05$ was considered statistically significant and significant level is indicated as follows: * $p < 0.05$, ** $p < 0.01$, *** $p < 0.001$. Specific details including the statistic test and the number of experimental replicates were demonstrated in figure legends.